Cu-Co mixed oxide catalysts for the total oxidation of toluene and propane

W. Zhang, C. Descorme, J. Valverde, A. Giroir-Fendler

Cu-Co mixed oxide catalysts for the total oxidation of toluene and propane

Weidong Zhang[a], Claude Descorme[a], Jose Luis Valverde[b], Anne Giroir-Fendler[a,*]

[a] Univ. Lyon, Université Claude Bernard Lyon 1, CNRS, IRCELYON, 2 avenue Albert Einstein, Villeurbanne, F-69622, France

[b] Department of Chemical Engineering, Faculty of Chemical Science and Technology, University of Castilla-La Mancha, Avenida Camilo José Cela 12, 13005, Ciudad Real, Spain

*Corresponding author: Anne Giroir-Fendler (e-mail: anne.giroir-fendler@ircelyon.univ-lyon1.fr)

Abstract

Cu-Co mixed oxides were fabricated via co-precipitation, characterized by TG/DTA, FTIR, ICP, XRD, Raman and CO-TPR, and tested in the total oxidation of toluene and propane. Adding an appropriate amount of copper to cobalt oxide caused structural defects and weakened the Co–O bond, thereby benefiting the activation of oxygen. Moreover, the reducibility of Co_3O_4 was greatly improved in the presence of copper. In terms of toluene oxidation, a promoting effect of Cu was observed in both activity and durability, which could be related to the enhanced redox ability induced by the strong Cu-Co interaction and the inhibitory effect of Cu on the accumulation of surface carbonaceous species, respectively. $Cu_{0.2}Co$ exhibited the best toluene oxidation performance (T_{90} =240 °C) and excellent long-term durability. On the other hand, in propane oxidation, the activity of the Cu-Co catalysts decreased dramatically as the copper content increased, due to the extremely low intrinsic activity of CuO. The effects of CO_2, water vapor and NO on propane oxidation over Co_3O_4 and $Cu_{0.2}Co$ were also examined.

Key words: Cu-Co mixed oxides; Cobalt oxide; Reducibility; Toluene oxidation; Propane oxidation.

1. Introduction

Atmospheric volatile organic compounds (VOCs), mainly originate from industrial

emissions, contribute to the formation of ozone and photochemical smog [1], which cause severe air pollution. Catalytic oxidation is an attractive technique to efficiently eliminate VOCs at low temperature, without generating secondary pollutants. Although noble metal catalysts show favorable activity in VOCs oxidation at low temperature, their high cost and other related issues (volatility, sintering and chlorine poisoning) restrict their large-scale application. Base metal oxides can be considered as good alternatives to noble metals since they are easily available, they have a higher thermal stability and a better resistance towards chloride poisoning. Among all non-noble metal oxides, which were extensively studied, Co_3O_4 turns to be one of the most promising catalysts for VOCs oxidation. In some VOCs oxidation, the activity of Co_3O_4 is comparable to that of noble metal catalysts [2,3].

To enhance the catalytic performance of Co_3O_4, a second component might be introduced to act as a promoter. As a result, the microstructure of Co_3O_4 can be tuned and heterogeneous interfaces can be created, promoting a synergistic effect between the different oxide phases when they are not fully miscible. Since a redox mechanism is involved in the total oxidation of VOCs [4,5], a second component improving the reducibility of the oxide phase is always preferred. Fierro et al. have evidenced that the reducibility of the Cu-Co mixed oxides was always promoted compared to Co_3O_4 due to the strong interaction between Co and Cu in such mixed oxide phases [6]. It has been recently reported that Cu-Co binary metal oxides show better performance over its individual components in the catalytic oxidation. For instance, CuO/Co_3O_4 composite oxides have been found to be more active than pure Co_3O_4 in the preferential oxidation of CO in a H_2-rich stream [7,8], in benzene oxidation [9] and in toluene oxidation [10] due to the synergistic effect between Cu and Co. In toluene oxidation, similar cooperation effects between Cu and Co oxides were also observed when they are supported on halloysite [11], sepiolite [12] or carbon [13]. Consequently, Cu-Co mixed oxide catalytic systems might be valuably developed to accelerate VOCs oxidation reactions.

In this study, Cu-Co mixed oxides were prepared by co-precipitation and used as catalysts in the total oxidation of toluene and propane, two representative molecules for aromatic and alkane hydrocarbons, respectively. The objective of the present work was to develop low-price, highly efficient and stable catalysts for VOCs oxidation.

2. Experimental

2.1. Catalyst preparation

Cobalt oxide, Cu-Co mixed oxides and copper oxide were prepared via carbonate-precipitation. Typically, 100 mL of a 0.2 M metal nitrate solution was mixed with 100 mL of a 0.22 M sodium carbonate solution. The pH of the solution was adjusted to 9.5, using sodium hydroxide, and maintained at this value at room temperature for 1 h under vigorous stirring. After centrifugation and washing with distilled water, the solid was dried at 80 ºC overnight and further calcined in flowing air at 500ºC for 2 h (2 ºC min^{-1}). The final products were referred to as Cu_xCo, where x is the Cu:Co atomic ratio.

2.2. Catalyst characterization

Thermogravimetry and differential thermal analysis (TG/DTA) was performed on a SETARAMSetsys Evolution 12 calorimeter. 5–7 mg of the metal precursor was heated in an air flow from 25 to 800 °C with a rate of 10 °C min^{-1}.

Fourier Transform infrared (FTIR) spectra were collected on a PerkinElmer FT-IR C92712 spectrometer in attenuated total reflectance mode.

The chemical composition of the oxides was determined by inductively coupled plasma optical emission spectroscopy (ICP-OES, Horiba Jobin Yvon). The oxides were pretreated by a solution containing H_2SO_4 and HNO_3 at ca. 400 °C.

X-ray diffraction (XRD) patterns were recorded on a Bruker D8 Advance diffractometer equipped with Cu Kα radiation (λ = 0.154184 nm). Samples were scanned in the 2-theta range from 10° to 80° using a step of 0.02° and counting time of 2 s per step.

Raman spectra were obtained on a Horiba LabRam HR spectrometer equipped with Ar^+ laser beam (λ = 514 nm).

N_2 adsorption–desorption isotherms were obtained at −196 °C on a Micromeritics TRISTAR II apparatus. Each sample was outgassed at 300 °C for 3 h before analysis. The specific surface area was determined by the standard Brunauer–Emmett–Teller (BET) equation, and the total pore volume and pore size distribution were calculated by the Barrett–Joyner–Halenda (BJH) method.

Temperature program reduction in CO (CO-TPR) was performed on a Micro-GC (SRA % GC-R3000). The sample (0.03 g) was pretreated at 300 °C in He for 0.5 h. After cooling down to 50 °C, the sample was treated by 0.3 vol. % CO/He gas mixture (100 mL min^{-1}), from 50 to 750 °C at a rate of 5 °C min^{-1}.

2.3. Catalytic activity test

The catalytic test was carried out in a U-shaped reactor (i.d. = 4 mm) using 0.15 g of catalyst (particle size of ca. 200 μm) mixed with ca. 0.7 g of silicon carbide (particle size of 150–300 μm). The mixture was packed over a quartz wool plug inside the reactor. The catalyst bed height was controlled at 6 mm. The reactant stream contained 1000 ppm of VOCs (toluene or propane), 21 vol.% O_2 and balanced N_2 (for toluene) or He (for propane), with a total flow rate of 100 mL min^{-1} (weight hourly space velocity (WHSV) = 40,000 mL g^{-1} h^{-1}). To evaluate the effect of CO_2, water vapor and NO on the reaction, 5.0 vol.% CO_2 and 500 ppm of NO were introduced from standard gas cylinder, whereas 5.0 vol.% H_2O was introduced by passing the reactant stream through a water saturator at a certain temperature.

In toluene oxidation tests, the reactant stream was fed into the reactor before being heated from room temperature to 150 °C (5 °C min^{-1}) and held at this temperature for 0.5 h to stabilize the system. Then, the temperature was increased from 150 °C to 350 °C (2 °C min^{-1}) and held at this temperature for 1 h. Next, the reactor was cooled down to 150 °C (5 °C min^{-1}). The concentrations of CO and CO_2 were monitored by an on-line Rosemount Xtreme Gas Infrared Analyzer (Emerson Electric Co.).

In propane oxidation tests, the reaction temperature program was analogous to that of toluene oxidation except that the temperature interval was 100–350 °C. An on-line micro gas chromatograph (SRA % GC-R3000) was used to monitor the gas effluents.

The conversion of toluene or propane to CO_2 was calculated as follows:

$$X_{C_7H_8}(\%) = \frac{[CO_2]}{7[C_7H_8]} \times 100$$

$$X_{C_3H_8}(\%) = \frac{[CO_2]}{3[C_3H_8]} \times 100$$

where $[CO_2]$, $[C_7H_8]$ and $[C_3H_8]$ are the outlet CO_2 concentration, the inlet toluene and propane concentration, respectively.

The toluene/propane oxidation reaction rate (r, mol s^{-1} g_{Co}^{-1}) based on the cobalt mass was calculated as follows:

$$r = \frac{X \cdot F}{m \cdot \omega}$$

where X is the conversion of toluene/propane to CO_2, F is the flow rate of toluene/propane (mol s^{-1}) in the inlet gas, m is the mass of the catalyst used (g) and ω is the mass ratio of cobalt in the catalyst determined by ICP-OES.

3. Results and Discussion

3.1. Decomposition of the oxide precursors and formation of the oxides

Fig. 1 shows the TG/DTA curves of the Cu-Co mixed oxide precursors. The weight loss below 150°C was attributed to the removal of water, whereas the weight loss from 150 to 500°C was due to the decomposition and oxidation of the oxide precursors to produce Co_3O_4 and CuO. As the copper content increased, the full decomposition temperature of the mixed oxide precursors shifted to higher region. Namely, the presence of copper somehow delayed the decomposition of the cobalt precursor. Indeed, looking at the DTA curves, two peaks were observed for the pure cobalt precursor, one endothermic and one exothermic. These two peaks shifted towards higher temperatures, being weakened and broadened when copper was introduced, confirming the inhibiting effect of copper on the decomposition of the cobalt precursor. In addition, the endothermic peak observed upon decomposition of the pure copper precursor did not appear upon decomposition of the mixed oxide precursors, further indicating a strong interaction effect between the two copper and cobalt phases.

FTIR spectra of the Cu-Co mixed oxide precursors are shown in **Fig. 2a**. Characteristic bands of the metal carbonate hydroxides are systematically observed. For all samples, bands at 2360 and 2343 cm^{-1} are due to atmospheric CO_2 and physically adsorbed CO_2 species, respectively [14]. For the pure cobalt precursor, a broad band characteristic of the stretching vibration modes of H_2O and O–H groups appeared at 3495 cm^{-1} [15–17]. In addition, bands at 952 and 515 cm^{-1} were assigned to δ(Co–OH) and ρ(Co–OH) [15–17]. Bands at 1445 ($\nu(OCO_2)$, $\nu(CO_3)$), 1068

(ν(C=O)), 828 (δ(CO_3)), 738 (δ(OCO)) and 668 cm^{-1} (ρ(OCO)) indicated the presence of carbonate anions [15–17]. In the case of the pure copper precursor, the bands at about ca. 3401, 3310, 1510, 1381, 1096, 867, 817, 746, 570, 522 and 426 cm^{-1} are typical of $CuCO_3 \cdot Cu(OH)_2$ [18]. The FTIR spectra of $Cu_{0.05}Co$ and $Cu_{0.2}Co$ are similar to that of pure cobalt precursor, whereas Cu_2Co exhibited an FTIR spectrum combining the characteristics of both cobalt and copper precursors.

After calcination at 500°C, all bands characteristic of metal carbonate hydroxides disappeared (**Fig. S1**). Simultaneously, new bands due to the formation of metal oxides emerged (**Fig. 2b**). Two bands at 656 and 553 cm^{-1} were observed for Co_3O_4, $Cu_{0.05}Co$ and $Cu_{0.2}Co$; corresponding to the Co–O vibration in the Co_3O_4 spinel structure [4,17]. The Co–O vibration band shifted towards lower wavenumbers as the copper content increased; indicating a decrease in the Co–O bond strength in Co_3O_4 [19] and evidencing some interactions between the two Cu and Co oxide phases [20]. It was previously reported that a reduced Co–O bond strength allows easier extraction of O from the surface of Co_3O_4, facilitating the formation of oxygen vacancy and promoting the redox ability [21]. Typical Cu–O vibration modes in CuO were observed at 595, 530, and 473 cm^{-1} [18,22]. Cu_2Co exhibited vibration bands corresponding to both oxides.

The chemical composition of the as-prepared oxides as determined by ICP (**Table 1**) was in good agreement with the theoretical one.

Fig. 3a shows the XRD patterns of the as-prepared oxides. Typical diffraction peaks attributed to the cubic Co_3O_4 spinel structure and the monoclinic tenorite CuO phase were observed for the pure cobalt and copper oxides, respectively. In the case of the Cu-Co mixed oxides, only the diffraction peaks ascribed to Co_3O_4 could be seen in $Cu_{0.05}Co$, whereas both diffraction peaks of Co_3O_4 and CuO were detected for $Cu_{0.2}Co$ and Cu_2Co. Considering the fact that Cu^{2+} and Co^{2+} have similar ionic radius, limited distortion of the crystalline structure are expected upon mixing. Indeed, the XRD patterns of Co_3O_4 and Cu-Co spinel are close. As a result, any definite conclusion on the formation of the Cu-Co spinel phase was hard to make. However, considering the fact that the main (311) diffraction line for the Co_3O_4 and all Cu-Co mixed oxide samples (**Fig. S2**) appeared at the exact same position, we could obviously conclude that the mixed spinel phase did not form. In parallel, when increasing the copper

content, the average crystallite size of the Co_3O_4 oxide phase was observed to decrease (**Table 1**). To explain the higher dispersion of Co_3O_4, CuO was proposed to be highly disperse on the surface of Co_3O_4, inhibiting the growth of the Co_3O_4 nanocrystals upon calcination [23,24].

Raman spectra were collected to further investigate the structural properties of the as-prepared oxides (**Fig. 3b**). Five bands (A_{1g} + E_g + $3F_{2g}$) corresponding to the Raman active modes of Co_3O_4 [2] and three bands ($2B_g$ + A_{1g}) characteristic of the Raman active modes of CuO [25] were observed for pure cobalt and copper oxide, respectively. For the Cu-Co mixed oxides, the Raman bands corresponding to Co_3O_4 were much broader and shifted to lower positions compared to the pure cobalt oxide. These modifications were attributed both to the size effect and to the occurrence of a more disordered structure [21,26]. In addition, upon Cu addition, the Raman symmetry changed for the Cu-Co mixed oxides, reflecting the change of the cobalt coordinative environment in the spinel structure induced by lattice distortion or residual stress [21]. $Cu_{0.2}Co$ appeared to have the most defective structure, as speculated from the largest red shift observed, which is conducive to the decrease of the Co–O bond strength and the formation of oxygen vacancy [21], which agrees well with the FTIR analysis. Weak Raman bands typical of CuO could also be seen for the Cu_2Co sample, which is in line with the XRD results.

Fig. S3 shows the N_2 adsorption–desorption isotherms and the pore size distributions of the Cu-Co mixed oxides. Type IV isotherms, with narrow hysteresis loops, were observed for all samples, suggesting a mesoporous structure. Mesoporosity is confirmed by the pore size distribution centered around 2.5 nm. Co_3O_4, $Cu_{0.05}Co$ and $Cu_{0.2}Co$ showed similar specific surface areas (**Table 1**, SSA, 39–43 $m^2\ g^{-1}$). CuO had the lowest SSA value of 5 $m^2\ g^{-1}$ and the SSA of Cu_2Co stood in the middle. The pore volume increased while the Cu:Co atomic ratio increased up to 0.2 and then decreased. $Cu_{0.2}Co$ possessed the largest pore volume (0.123 $cm^3\ g^{-1}$).

3.2. Reducibility

The reducibility of the Cu-Co mixed oxides was investigated by performing CO-TPR experiments. **Fig. 4** shows the CO consumption and CO_2 production curves. The CO_2 production matched well with the CO consumption. As can be seen, all samples mainly exhibited two CO_2 production peaks, both below 600°C. For pure

Co_3O_4, the two peaks correspond to the stepwise reduction of Co_3O_4 to metallic Co, which proceeds via CoO intermediate, while for pure CuO, the ones could be assigned to the reduction of Cu^{2+} into Cu^0. The total CO_2 production (**Table S1**) suggested in all cases the complete reduction of the oxides to the corresponding metal. The first reduction peak shifted towards lower temperatures when increasing the copper content. Pure Co and Cu oxides showed higher reduction temperatures compared to the Cu-Co mixed oxides. Considering the onset reduction temperature (the temperature when more than 100 ppm of CO_2 were produced, **Table S1**), the samples ranked as follows: Cu_2Co < $Cu_{0.2}Co$ < $Cu_{0.05}Co$ < Co_3O_4 < CuO; Cu_2Co starting to be reduced at the lowest temperature (91°C). The interaction between Co_3O_4 and CuO led to an enhanced reducibility of the cobalt species, which is consistent with the results reported earlier by Fierro et al. [6].

3.3. Catalytic performance

The catalytic performance of the as-prepared samples was evaluated in the total oxidation of two representative VOCs: toluene and propane. Light-off curves represent the evolution of the CO_2 yield with reaction temperature during the cooling ramp. The temperatures at 10, 50 and 90% of toluene/propane conversion to CO_2 were defined as T_{10}, T_{50} and T_{90}, respectively.

3.3.1. Toluene oxidation

Fig. 5a shows the evolution of the toluene conversion to CO_2 as a function of temperature. CuO exhibited much poorer catalytic performance compared to Co_3O_4. The T_{90} value for CuO was above 350°C, while it was 267°C for Co_3O_4 (**Table S2**). The catalytic performance of the Cu-Co mixed oxides was superior to that of the single oxides. Among the Cu-Co mixed oxides, $Cu_{0.2}Co$ exhibited the highest catalytic performance, with a reaction initiation temperature of 175°C and a full-conversion temperature of 257°C.

To better compare the catalytic activity of the cobalt-containing catalysts, the toluene oxidation rate was calculated and normalized to the mass of cobalt in the oxide. The data obtained while the conversion is lower than 20% (kinetic regime) are plotted in **Fig. S4a**. $Cu_{0.2}Co$ appeared to be the most active catalyst in the oxidation of toluene, which was attributed to the abundance of surface vacancy and enhanced reducibility of Co_3O_4 induced by the synergistic effect between Co_3O_4 and CuO.

Though Cu_2Co had better reducibility compared to $Cu_{0.2}Co$, it contains about 2/3 of CuO in its structure. As discussed above, CuO can provide fewer active sites compared with Co_3O_4. In addition, the excess amount of CuO on the surface may even block the active sites of Co_3O_4, thus the abundance of less active CuO in Cu_2Co limited its performance.

A comparison between the toluene oxidation performance of the optimal catalyst $Cu_{0.2}Co$ and similar catalysts recently reported was made (**Table 2**). $Cu_{0.2}Co$ showed performance better than Co_3O_4 microsphere [27], Co_3O_4-cube [28] and $CeCoO_x$-MNS [29], similar to Mn2Co1 oxides [30], $Mn_{2.4}Fe_{0.6}O_4$ [31] and 3Mn1Ce [32], and slightly inferior to AT-CuMn-S [33]. It should be noted that some of the above reported catalysts require hydrothermal condition [27,28], long operating time [30] costly organic compounds [29] or acid treatment [33], while the synthesis of $Cu_{0.2}Co$ in this work is low-cost, simple, fast, and has potential for large-scale production.

Considering that the Co_3O_4 crystallites could sinter upon reaction [34,35], the fresh Co_3O_4 and $Cu_{0.2}Co$ catalysts were treated in flowing air at 700°C for 1 h to simulate thermal ageing upon reaction. **Fig. S5** shows that thermal ageing resulted in a significant shift of the light-off curves towards higher temperatures. The T_{50} conversion value for Co_3O_4 increased from 239 to 259°C whereas for $Cu_{0.2}Co$ this parameter shifted from 216 to 269°C. The deactivation observed for $Cu_{0.2}Co$ was much more severe, which could be attributed to both the sintering of the Co_3O_4 phase and to the segregation of CuO phase, destroying a possible synergetic effect between the two oxide phases.

The cycling stability of $Cu_{0.2}Co$ upon toluene oxidation was tested. Consistent results were obtained throughout three successive catalytic cycles (**Fig. S6**), evidencing the excellent cycling stability of this catalyst.

The long-term durability of $Cu_{0.2}Co$ at both high and low toluene conversions was also investigated and compared with that of Co_3O_4. As can be seen from **Fig. 6**, toluene conversion over $Cu_{0.2}Co$ decreased from ca. 60 (initial conversion) to 52% during the first 7 h on stream before stabilizing for the rest of the catalytic test. By removing toluene from the feed for about 0.5 h, the initial activity of the $Cu_{0.2}Co$ catalyst could be transiently restored. In comparison, the initial activity loss observed in the case of Co_3O_4 was much severe, with a drastic drop of the toluene conversion from ca. 60 to

6%. Deactivation was also reversible in the case of Co_3O_4. **Fig. S7a** shows that when starting from the similar toluene conversion of 11%, 8% of the conversion can be maintained over $Cu_{0.2}Co$ after 24 h, whereas only 2% of conversion left in the same condition over Co_3O_4. Anyway, $Cu_{0.2}Co$ presented a much higher catalytic durability in the oxidation of toluene than Co_3O_4.

Generally speaking, the deactivation of a catalyst can be related to phase/structure changes, particle sintering, coke deposition and/or change in surface composition [36]. Toluene oxidation is a two-step process including partial oxidation of toluene to some intermediates (benzyl alcohol, benzaldehyde benzoic acid, and benzene etc.) at low temperatures and further oxidation of these intermediates to CO_2 at high temperatures [37]. In our case, on the one hand, a large amount of CO_2 was produced during the heating ramp (**Fig. S8**), greatly exceeds the theoretical value of 7000 ppm, indicating abundant accumulation of intermediates on the surface of the catalyst at low temperature. On the other hand, once the toluene feed was cut off after a long-term toluene oxidation test, much CO_2 production was observed in 10 min (**Fig. S9**), which could be attributed to the decomposition of the intermediates; Hereafter, the catalytic performance was recovered (**Fig. 6**). Based on the results above, we speculate that toluene is readily adsorbed and bound on the surface of the catalysts at low temperatures, forming some intermediates that require a higher temperature to be oxidized. The accumulated intermediates would saturate the active surface, causing a decrease of catalytic activity [38].

In order to understand the reason for the better long-term toluene oxidation durability of $Cu_{0.2}Co$, the used catalysts after a heating-cooling catalytic cycle were further treated in air flow to achieve temperature programmed oxidation of the surface. The CO_2 evolution during this period was recorded and showed in **Fig. 7**. As one can see, the yielded CO_2 over Co_3O_4 was much higher than that over CuO. The addition of Cu into Co_3O_4 seems to hinder the accumulation of toluene or carbonaceous intermediates onto the surface of the catalysts; the more Cu added, the less amount of CO_2 was produced over the mixed Cu-Co oxides. The results well explain the observed significantly different durability of Co_3O_4 and $Cu_{0.2}Co$ in toluene oxidation. The deposition of carbonaceous species on the surface of Co_3O_4 can block some active sites, thereby deactivating the performance, whereas the facile desorption of toluene or reaction intermediates from the surface of $Cu_{0.2}Co$ may be responsible for its decent

toluene oxidation durability.

3.3.2. Propane oxidation

The evolution of the propane conversion to CO_2 as a function of temperature is shown in **Fig. 5b** for the different oxide catalysts. CuO was a very poor catalyst in the oxidation of propane; only 22% of propane was converted into CO_2 at 350°C. In contrast, Co_3O_4 exhibited excellent propane oxidation performance, with a conversion over 99% at 243°C. The catalytic performance of the Cu-Co mixed oxides laid somewhere in between the one of the single oxides. The performance of the Cu-Co mixed oxides decreased with increasing the copper content. The same trend is observed when the propane oxidation rate is expressed per gram of cobalt (**Fig. S4b**). In conclusion, pure Co_3O_4 was the best catalyst in propane oxidation, Cu exerts a detrimental effect on the catalytic performance. Nevertheless, full conversion of propane can be still achieved over $Cu_{0.2}Co$ at a temperature of 290 °C. As reported earlier by different authors [39–41], the different catalytic performance of the Cu-Co mixed oxides in toluene and propane oxidation may be ascribed to the different types of C–C bonds in these two molecules, and the different rate-determining steps for both reaction mechanisms. For example, García [39] observed different performance trends for propane and naphthalene oxidation over a series of metal oxide catalysts. Aparicio [40] reported that the oxidation performance of CoO_x/SiO_2 catalysts for propane varied that for aromatic hydrocarbons. Similarly, Solsona [41] found inconsistent performance of α-Fe_2O_3 catalysts in the total oxidation of propane and toluene. They assumed the reduction step as the limiting step of propane oxidation via a Mars–Van Krevelen mechanism, while stressing the importance of the accessibility of the toluene molecules to the adsorption sites in the oxidation of toluene via a Rideal–Eley mechanism. Moreover, as showed in **Fig. 5**, the light-off curve gap between CuO and Co_3O_4 for propane oxidation was much bigger than that for toluene oxidation. Therefore, CuO species dispersed on the surface of Co_3O_4 can have a poisoning effect for propane oxidation by covering/blocking some active sites of Co_3O_4, resulting in poor ability to oxidize propane.

The propane oxidation reaction over $Cu_{0.2}Co$ was repeated, with the reaction temperature increased up to 350 ºC and then cooled down to 100 ºC for three times. The light-off curves barely changed (**Fig. S6b**). The long-term durability of $Cu_{0.2}Co$ and

Co_3O_4 for propane oxidation was also tested. As shown in **Fig. S7b**, again, $Cu_{0.2}Co$ exhibited a better durability with respect to Co_3O_4, after continuous running for more than 55 h, the conversion over $Cu_{0.2}Co$ reduced slightly from 21% to 19%, while Co_3O_4 decreased its initial conversion from 24% to 18%. It seems that the intermediates can be converted to CO_2 fleetly over $Cu_{0.2}Co$, preventing the blockage of active sites, thereby retaining a stable performance. Additionally, the durability of $Cu_{0.2}Co$ and Co_3O_4 in the absence or presence of CO_2, NO and H_2O was studied (**Fig. 8**). For both catalysts, the introduction of CO_2 or H_2O caused an obvious reduction in propane conversion, which could be totally recovered by cutting off CO_2 or H_2O feed, indicating the reversibility of the inhibition effect. However, the addition of NO led to severely deactivation of the catalysts, which was partially irreversible. The deactivation was much more evident for Co_3O_4 than for $Cu_{0.2}Co$. The conversion loss of $Cu_{0.2}Co$ was 7% while that of Co_3O_4 was 19%. Therefore, $Cu_{0.2}Co$ was more durable in the presence of NO than Co_3O_4.

4. Conclusions

Cu-Co mixed oxides were prepared via co-precipitation and compared with single Co_3O_4 in the total oxidation of toluene and propane. All Cu-Co catalysts showed enhanced toluene oxidation performance with respect to single Co_3O_4, among which $Cu_{0.2}Co$ stood out. The characterization results suggest that $Cu_{0.2}Co$ possesses the largest pore volume (easy access to toluene adsorption), the most defective structure and the weakest Co–O bond strength (rich surface adsorbed oxygen species), as well as excellent low temperature reducibility (high lattice oxygen mobility). All these characteristics contribute to its superior performance in toluene oxidation. In contrast, All Cu-Co catalysts were inferior to single Co_3O_4 in the total oxidation of propane, the more Cu content, the worse performance, which could be associated with the low intrinsic activity of CuO for propane oxidation. On the other hand, $Cu_{0.2}Co$ demonstrated excellent cycling stability and long-term durability in both toluene and propane oxidation, whereas Co_3O_4 deactivated severely in toluene oxidation due to the accumulation of carbonaceous intermediates. In addition, $Cu_{0.2}Co$ and Co_3O_4 presented decent propane oxidation durability under dry condition, reversible deactivation in 5 vol.% CO_2 or 5 vol.% H_2O, whereas partially irreversible deactivation in the presence of 500 ppm of NO.

Acknowledgements

This work was financially supported by the region Auvergne Rhone Alpes (PAI contract number 1900797501 – 10687), the University Claude Bernard Lyon 1 and the CNRS. We gratefully acknowledge the China Scholarship Council of P.R. China for ZHANG Weidong's grant.

References

[1] C. He, J. Cheng, X. Zhang, M. Douthwaite, S. Pattisson, Z. Hao, Recent Advances in the Catalytic Oxidation of Volatile Organic Compounds: A Review Based on Pollutant Sorts and Sources, Chem. Rev. 119 (2019) 4471–4568. doi:10.1021/acs.chemrev.8b00408.

[2] W. Tang, W. Xiao, S. Wang, Z. Ren, J. Ding, P.-X. Gao, Boosting catalytic propane oxidation over PGM-free Co3O4 nanocrystal aggregates through chemical leaching: A comparative study with Pt and Pd based catalysts, Appl. Catal. B Environ. 226 (2018) 585–595. doi:10.1016/j.apcatb.2017.12.075.

[3] S. Mo, Q. Zhang, Y. Sun, M. Zhang, J. Li, Q. Ren, M. Fu, J. Wu, L. Chen, D. Ye, Gaseous CO and toluene co-oxidation over monolithic core-shell Co3O4-based hetero-structured catalysts, J. Mater. Chem. A. 7 (2019) 16197–16210. doi:10.1039/c9ta03750k.

[4] J. Gonzalez-Prior, J.I. Gutierrez-Ortiz, R. Lopez-Fonseca, G. Busca, E. Finocchio, B. De Rivas, Oxidation of chlorinated alkanes over Co3O4/SBA-15 catalysts. Structural characterization and reaction mechanism, Catal. Sci. Technol. 6 (2016) 5618–5630. doi:10.1039/c6cy00321d.

[5] L.F. Liotta, H. Wu, G. Pantaleo, A.M. Venezia, Co3O4 nanocrystals and Co3O4–MOx binary oxides for CO, CH4 and VOC oxidation at low temperatures: a review, Catal. Sci. Technol. 3 (2013) 3085. doi:10.1039/c3cy00193h.

[6] G. Fierro, M. Lo Jacono, M. Inversi, R. Dragone, P. Porta, TPR and XPS study of cobalt–copper mixed oxide catalysts: evidence of a strong Co–Cu interaction, Top. Catal. 10 (2000) 39–48. doi:10.1023/A:1019151731177.

[7] D. Li, X. Liu, Q. Zhang, Y. Wang, H. Wan, Cobalt and copper composite oxides as efficient catalysts for preferential oxidation of CO in H2-Rich stream, Catal. Letters. 127 (2009) 377–385. doi:10.1007/s10562-008-9693-0.

[8] S. Varghese, M.G. Cutrufello, E. Rombi, C. Cannas, R. Monaci, I. Ferino, CO oxidation and preferential oxidation of CO in the presence of hydrogen over SBA-15-templated CuO-Co3O4 catalysts, Appl. Catal. A Gen. 443–444 (2012) 161–170. doi:10.1016/j.apcata.2012.07.038.

[9] S. Li, H. Wang, W. Li, X. Wu, W. Tang, Y. Chen, Effect of Cu substitution on promoted benzene oxidation over porous CuCo-based catalysts derived from layered double hydroxide with resistance of water vapor, Appl. Catal. B Environ. 166–167 (2015) 260–269. doi:10.1016/j.apcatb.2014.11.040.

[10] L. Jia, Y. Guo, T.P. Tran, M. Sakurai, H. Kameyama, Synergistic Effect of Copper and Cobalt in Cu-Co Bulk Oxide Catalyst for Catalytic Oxidation of Volatile Organic Compounds, J. Chem. Eng. JAPAN. 45 (2012) 590–596. doi:10.1252/jcej.11we239.

[11] A.M. Carrillo, J.G. Carriazo, Cu and Co oxides supported on halloysite for the total oxidation of toluene, Appl. Catal. B Environ. 164 (2015) 443–452. doi:10.1016/j.apcatb.2014.09.027.

[12] M.B. Ardakani, H.A. Mahabadi, A.J. Jafari, Removal of toluene from air streams by cobalt-copper bimetallic catalysts supported on sepiolite, Toxicol. Environ. Chem. 101 (2019) 228–243. doi:10.1080/02772248.2019.1692018.

[13] J.-R. Li, F.-K. Wang, C. He, C. Huang, H. Xiao, Catalytic total oxidation of toluene over carbon-supported Cu-Co oxide catalysts derived from Cu-based metal organic framework, Powder Technol. 363 (2020) 95–106. doi:10.1016/j.powtec.2019.12.060.

[14] S.U. Rege, R.T. Yang, A novel FTIR method for studying mixed gas adsorption at low concentrations: H2O and CO2 on NaX zeolite and γ-alumina, Chem. Eng. Sci. 56 (2001) 3781–3796. doi:10.1016/S0009-2509(01)00095-1.

[15] D. Klissurski, E. Uzunova, Synthesis of nickel cobaltite spinel from coprecipitated nickel-cobalt hydroxide carbonate, Chem. Mater. 3 (1991) 1060–1063. doi:10.1021/cm00018a021.

[16] R. Xu, H.C. Zeng, Dimensional Control of Cobalt-hydroxide-carbonate Nanorods

and Their Thermal Conversion to One-Dimensional Arrays of Co3O4 Nanoparticles, J. Phys. Chem. B. 107 (2003) 12643–12649. doi:10.1021/jp035751c.

[17] Y. Wang, Y. Lei, J. Li, L. Gu, H. Yuan, D. Xiao, Synthesis of 3D-Nanonet Hollow Structured Co3O4 for High Capacity Supercapacitor, ACS Appl. Mater. Interfaces. 6 (2014) 6739–6747. doi:10.1021/am500464n.

[18] T.X. Wang, S.H. Xu, F.X. Yang, Green synthesis of CuO nanoflakes from CuCO3·Cu(OH)2 powder and H2O2 aqueous solution, Powder Technol. 228 (2012) 128–130. doi:10.1016/j.powtec.2012.05.007.

[19] Z. Zhu, G. Lu, Z. Zhang, Y. Guo, Y. Guo, Y. Wang, Highly Active and Stable Co3O4/ZSM-5 Catalyst for Propane Oxidation: Effect of the Preparation Method, ACS Catal. 3 (2013) 1154–1164. doi:10.1021/cs400068v.

[20] Y. Wang, X. Hu, K. Zheng, X. Wei, Y. Zhao, Effect of SnO2 on the structure and catalytic performance of Co3O4 for N2O decomposition, Catal. Commun. 111 (2018) 70–74. doi:10.1016/j.catcom.2018.04.004.

[21] Y. Lou, J. Ma, X. Cao, L. Wang, Q. Dai, Z. Zhao, Y. Cai, W. Zhan, Y.Y. Guo, P. Hu, G. Lu, Y.Y. Guo, Promoting Effects of In2O3 on Co3O4 for CO Oxidation: Tuning O2 Activation and CO Adsorption Strength Simultaneously, ACS Catal. 4 (2014) 4143–4152. doi:10.1021/cs501049r.

[22] L. Chen, L. Li, G. Li, Synthesis of CuO nanorods and their catalytic activity in the thermal decomposition of ammonium perchlorate, J. Alloys Compd. 464 (2008) 532–536. doi:10.1016/j.jallcom.2007.10.058.

[23] C. Wang, Q. Cheng, X. Wang, K. Ma, X. Bai, S. Tan, Y. Tian, T. Ding, L. Zheng, J. Zhang, X. Li, Enhanced catalytic performance for CO preferential oxidation over CuO catalysts supported on highly defective CeO2 nanocrystals, Appl. Surf. Sci. 422 (2017) 932–943. doi:10.1016/j.apsusc.2017.06.017.

[24] Z. Pu, Y. Liu, H. Zhou, W. Huang, Y. Zheng, X. Li, Catalytic combustion of lean methane at low temperature over ZrO2-modified Co3O4 catalysts, Appl. Surf. Sci. 422 (2017) 85–93. doi:10.1016/j.apsusc.2017.05.231.

[25] J.F. Xu, W. Ji, Z.X. Shen, W.S. Li, S.H. Tang, X.R. Ye, D.Z. Jia, X.Q. Xin, Raman spectra of CuO nanocrystals, J. Raman Spectrosc. 30 (1999) 413–415.

doi:10.1002/(SICI)1097-4555(199905)30:5<413::AID-JRS387>3.0.CO;2-N.

[26]J. González-Prior, R. López-Fonseca, J.I. Gutiérrez-Ortiz, B. de Rivas, Oxidation of 1,2-dichloroethane over nanocube-shaped Co3O4 catalysts, Appl. Catal. B Environ. 199 (2016) 384–393. doi:10.1016/j.apcatb.2016.06.046.

[27]F. Wang, H. Dai, J. Deng, S. Xie, H. Yang, W. Han, Nanoplate-aggregate Co3O4 microspheres for toluene combustion, Chinese J. Catal. 35 (2014) 1475–1481. doi:10.1016/S1872-2067(14)60072-3.

[28]Q. Ren, S. Mo, R. Peng, Z. Feng, M. Zhang, L. Chen, M. Fu, J. Wu, D. Ye, Controllable synthesis of 3D hierarchical Co3O4 nanocatalysts with various morphologies for the catalytic oxidation of toluene, J. Mater. Chem. A. 6 (2018) 498–509. doi:10.1039/C7TA09149D.

[29]F. Dong, W. Han, Y. Guo, W. Han, Z. Tang, CeCoOx-MNS catalyst derived from three-dimensional mesh nanosheet Co-based metal–organic frameworks for highly efficient catalytic combustion of VOCs, Chem. Eng. J. 405 (2021) 126948. doi:10.1016/j.cej.2020.126948.

[30]P. Wang, J. Wang, X. An, J. Shi, W. Shangguan, X. Hao, G. Xu, B. Tang, A. Abudula, G. Guan, Generation of abundant defects in Mn-Co mixed oxides by a facile agar-gel method for highly efficient catalysis of total toluene oxidation, Appl. Catal. B Environ. 282 (2021) 119560. doi:10.1016/j.apcatb.2020.119560.

[31]L. Liu, J. Sun, J. Ding, Y. Zhang, T. Sun, J. Jia, Highly Active Mn3–xFexO4 Spinel with Defects for Toluene Mineralization: Insights into Regulation of the Oxygen Vacancy and Active Metals, Inorg. Chem. 58 (2019) 13241–13249. doi:10.1021/acs.inorgchem.9b02105.

[32]J. Chen, X. Chen, X. Chen, W. Xu, Z. Xu, H. Jia, J. Chen, Homogeneous introduction of CeOy into MnOx-based catalyst for oxidation of aromatic VOCs, Appl. Catal. B Environ. 224 (2018) 825–835. doi:10.1016/j.apcatb.2017.11.036.

[33]Z. Ye, J.M. Giraudon, N. Nuns, G. Abdallah, A. Addad, R. Morent, N. De Geyter, J.F. Lamonier, Preferential dissolution of copper from Cu-Mn oxides in strong acid medium: Effect of the starting binary oxide to get new efficient copper doped MnO2 catalysts in toluene oxidation, Appl. Surf. Sci. 537 (2021) 147993. doi:10.1016/j.apsusc.2020.147993.

[34] L.F. Liotta, G. Di Carlo, G. Pantaleo, A.M. Venezia, G. Deganello, Co3O4/CeO2 composite oxides for methane emissions abatement: Relationship between Co3O4–CeO2 interaction and catalytic activity, Appl. Catal. B Environ. 66 (2006) 217–227. doi:10.1016/j.apcatb.2006.03.018.

[35] L.F. Liotta, G. Di Carlo, G. Pantaleo, G. Deganello, Catalytic performance of Co3O4/CeO2 and Co3O4/CeO2-ZrO2 composite oxides for methane combustion: Influence of catalyst pretreatment temperature and oxygen concentration in the reaction mixture, Appl. Catal. B Environ. 70 (2007) 314–322. doi:10.1016/j.apcatb.2005.12.023.

[36] Y. Zhang, Y. Liu, S. Xie, H. Huang, G. Guo, H. Dai, J. Deng, Supported ceria-modified silver catalysts with high activity and stability for toluene removal, Environ. Int. 128 (2019) 335–342. doi:10.1016/j.envint.2019.04.062.

[37] Z. Wang, H. Yang, R. Liu, S. Xie, Y. Liu, H. Dai, H. Huang, J. Deng, Probing toluene catalytic removal mechanism over supported Pt nano- and single-atom-catalyst, J. Hazard. Mater. 392 (2020) 122258. doi:10.1016/j.jhazmat.2020.122258.

[38] Y. Liu, H. Zhou, R. Cao, X. Liu, P. Zhang, J. Zhan, L. Liu, Facile and green synthetic strategy of birnessite-type MnO2 with high efficiency for airborne benzene removal at low temperatures, Appl. Catal. B Environ. 245 (2019) 569–582. doi:10.1016/j.apcatb.2019.01.023.

[39] T. García, B. Solsona, S.H. Taylor, Naphthalene total oxidation over metal oxide catalysts, Appl. Catal. B Environ. 66 (2006) 92–99. doi:10.1016/j.apcatb.2006.03.003.

[40] M.S.L. Aparicio, I.D. Lick, Total oxidation of propane and naphthalene from emission sources with supported cobalt catalysts, React. Kinet. Mech. Catal. 119 (2016) 469–479. doi:10.1007/s11144-016-1052-3.

[41] B. Solsona, T. García, R. Sanchis, M.D. Soriano, M. Moreno, E. Rodríguez-Castellón, S. Agouram, A. Dejoz, J.M. López Nieto, Total oxidation of VOCs on mesoporous iron oxide catalysts: Soft chemistry route versus hard template method, Chem. Eng. J. 290 (2016) 273–281. doi:10.1016/j.cej.2015.12.109.

Figure captions

Fig. 1. (a) TG and (b) DTA curves for the decomposition of the Cu-Co mixed precursors in air.

Fig. 2. FTIR spectra of the Cu-Co mixed (a) precursors and (b) oxides.

Fig. 3. (a) XRD patterns and (b) Raman spectra of the Cu-Co mixed oxides.

Fig. 4. (a) CO consumption and (b) CO_2 production in CO-TPR profiles for the Cu-Co mixed oxides.

Fig. 5. Light-off curves upon (a) toluene and (b) propane oxidation over the Cu-Co mixed oxides (reaction conditions: toluene/propane concentration = 1000 ppm, O_2 concentration = 21 vol.% and WHSV = 40,000 mL h^{-1} g^{-1}).

Fig. 6. Long-term durability test over Co_3O_4 and $Cu_{0.2}Co$ for toluene oxidation (reaction conditions: toluene concentration = 1000 ppm, O_2 concentration = 21 vol.% and WHSV = 40,000 mL h^{-1} g^{-1}).

Fig. 7. CO_2 evolution as a function of temperature in air flow after one heating-cooling cycle of toluene oxidation test over Cu-Co mixed oxides.

Fig. 8. Effect of 5 vol.% CO_2, 500 ppm of NO or 5 vol.% H_2O on the long-term durability of Co_3O_4 and $Cu_{0.2}Co$ for propane oxidation (reaction conditions: propane concentration = 1000 ppm, O_2 concentration = 21 vol.% and WHSV = 40,000 mL h^{-1} g^{-1}).

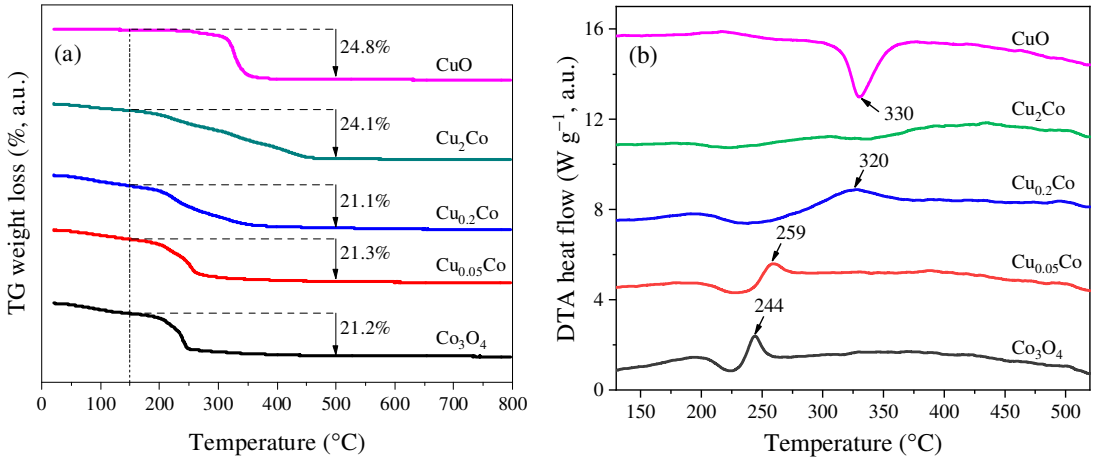

Fig. 1. (a) TG and (b) DTA curves for the decomposition of the Cu-Co mixed precursors in air.

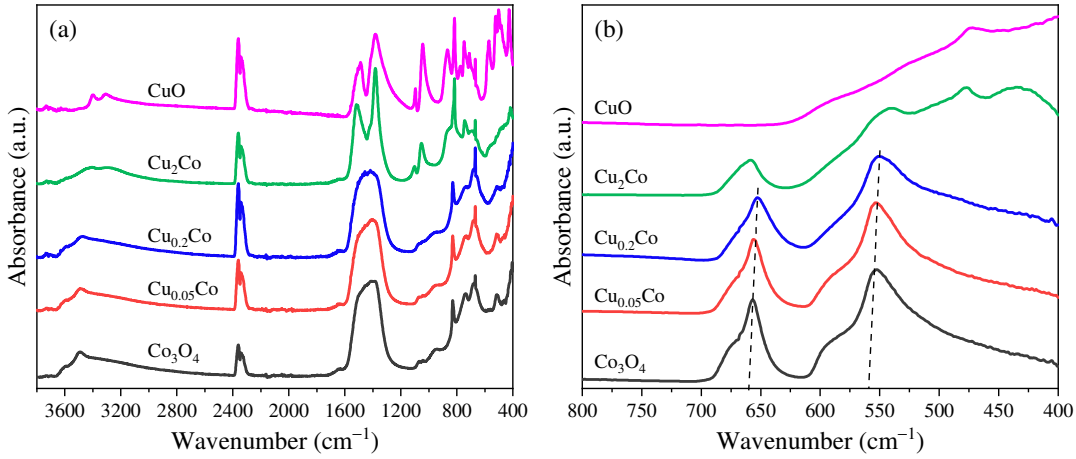

Fig. 2. FTIR spectra of the Cu-Co mixed (a) precursors and (b) oxides.

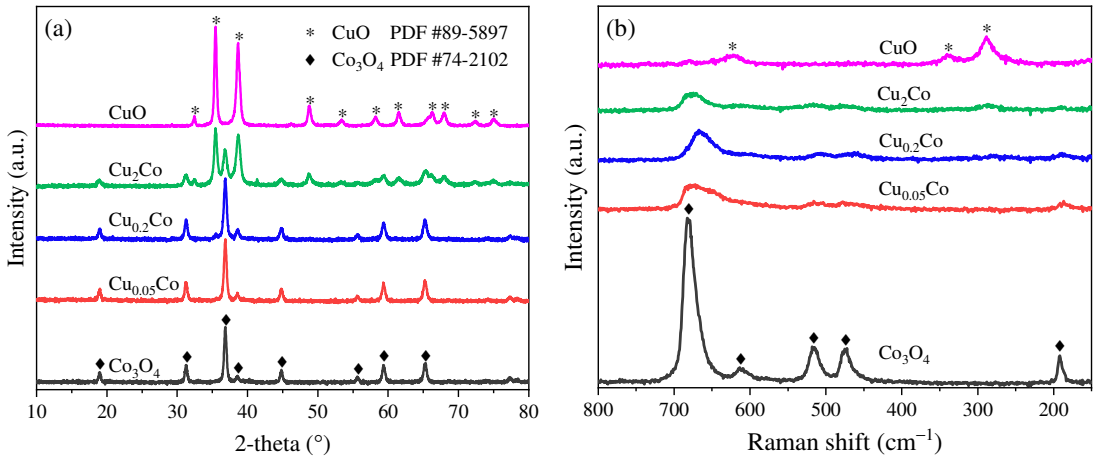

Fig. 3. (a) XRD patterns and (b) Raman spectra of the Cu-Co mixed oxides.

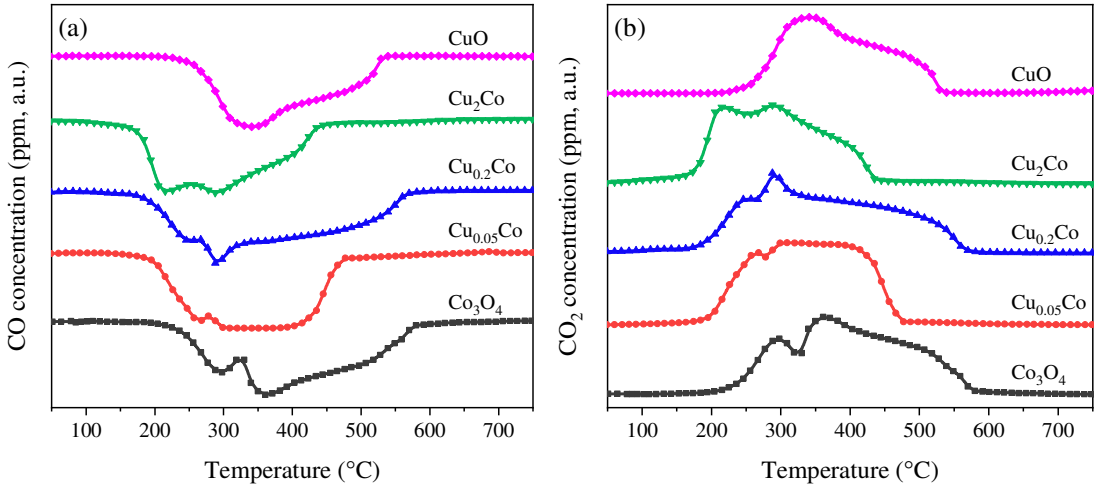

Fig. 4. (a) CO consumption and (b) CO_2 production in CO-TPR profiles for the Cu-Co mixed oxides.

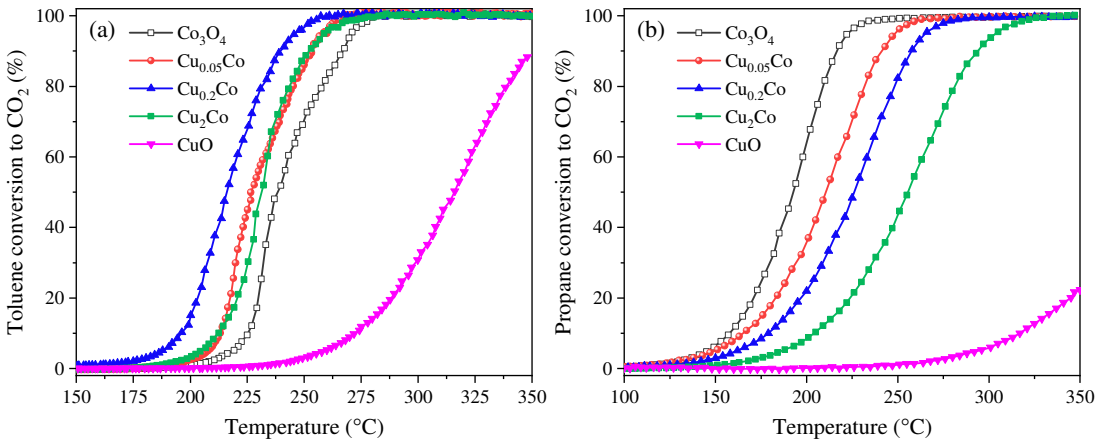

Fig. 5. Light-off curves upon (a) toluene and (b) propane oxidation over the Cu-Co mixed oxides (reaction conditions: toluene/propane concentration = 1000 ppm, O_2 concentration = 21 vol.% and WHSV = 40,000 mL h^{-1} g^{-1}).

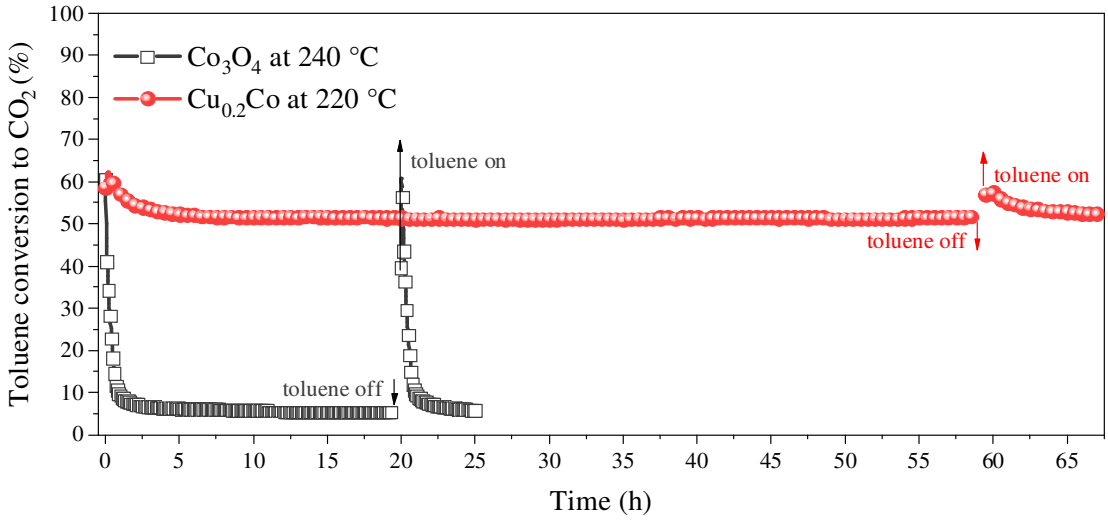

Fig. 6. Long-term durability test over Co_3O_4 and $Cu_{0.2}Co$ for toluene oxidation (reaction conditions: toluene concentration = 1000 ppm, O_2 concentration = 21 vol.% and WHSV = 40,000 mL h^{-1} g^{-1}).

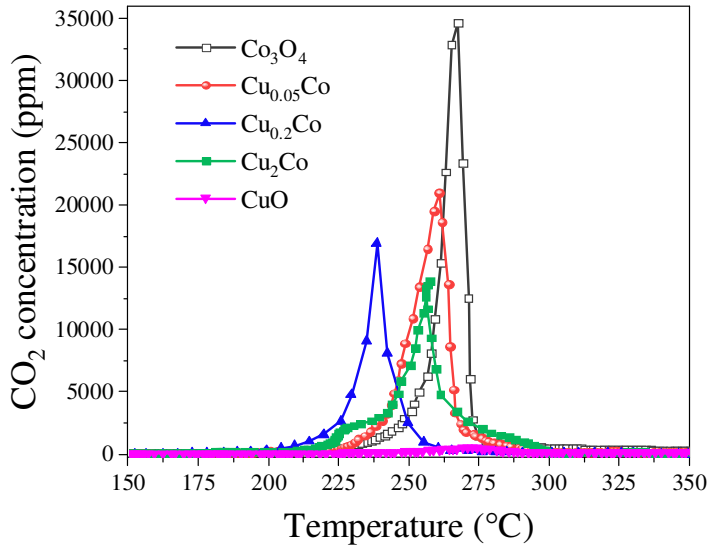

Fig. 7. CO_2 evolution as a function of temperature in air flow after one heating-cooling cycle of toluene oxidation test over Cu-Co mixed oxides.

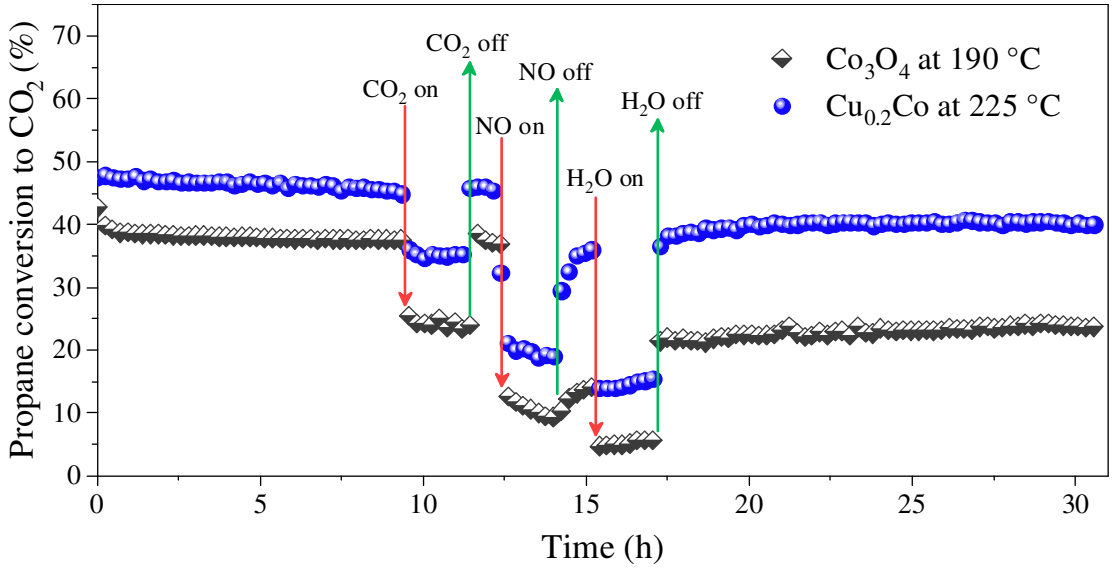

Fig. 8. Effect of 5 vol.% CO_2, 500 ppm of NO or 5 vol.% H_2O on the long-term durability of Co_3O_4 and $Cu_{0.2}Co$ for propane oxidation (reaction conditions: propane concentration = 1000 ppm, O_2 concentration = 21 vol.% and WHSV = 40,000 mL h^{-1} g^{-1}).

Table 1. Chemical composition, average crystallite size and textural data of the Cu-Co mixed oxides.

Catalysts	Cu/Co at.%	Cu wt.%	Co wt.%	d (nm)[a]	SSA ($m^2\ g^{-1}$)[b]	V_p ($cm^3\ g^{-1}$)[b]
Co_3O_4	-	-	70.1	22.3	41	0.092
$Cu_{0.05}Co$	0.05	3.6	66.2	20.3	43	0.120
$Cu_{0.2}Co$	0.19	12.1	58.1	18.5	39	0.123
Cu_2Co	1.98	48.8	22.9	13.4	29	0.057
CuO	-	72.9	-	-	5	0.028

[a] Average crystallite sizes calculated from XRD by Scherrer equation basing on (311) peak.

[b] Specific surface areas and total pore volumes obtained from N_2 adsorption isotherms.

Table 2. Survey of literature data on the catalytic oxidation of toluene over cobalt oxides or mixed metal oxides.

Catalyst	Reactant composition	WHSV ($mL\ h^{-1}\ g^{-1}$)	T_{90} (°C)	Ref.
Co_3O_4 microsphere	0.1% C_7H_8 + 40% O_2	20,000	254	[27]
Co_3O_4-cube	0.1% C_7H_8 + 20% O_2	48,000	248	[28]
$CeCoO_x$-MNS	0.3% C_7H_8 + 21% O_2	30,000	249	[29]
Mn2Co1 oxides	0.1% C_7H_8 + 20% O_2	60,000	236	[30]
$Mn_{2.4}Fe_{0.6}O_4$	0.1% C_7H_8 + 21% O_2	60,000	237	[31]
3Mn1Ce	0.1% C_7H_8 + 21% O_2	60,000	239	[32]
AT-CuMn-S	0.1% C_7H_8 + 21% O_2	30,000	232	[33]
$Cu_{0.2}Co$	0.1% C_7H_8 + 21% O_2	40,000	240	This work

Graphical Abstract